PERGAMON

Atmospheric Environment 33 (1999) 2157–2168

ATMOSPHERIC ENVIRONMENT

Effects of variable wind speed and direction on radon transport from soil into buildings: model development and exploratory results

W.J. Riley[a,*], A.L. Robinson[b,1], A.J. Gadgil[c], W.W. Nazaroff[d]

[a]*Department of Environmental Science, Policy, and Management, Ecosystem Sciences Division, University of California, Berkeley, CA 94720, USA*

[b]*Combustion Research Facility, Sandia National Laboratory, Livermore, CA, 94551, USA*

[c]*Indoor Environment Program, Lawrence Berkeley National Laboratory, Berkeley, CA 94720, USA*

[d]*Department of Civil and Environmental Engineering, University of California, Berkeley, CA 94720, USA*

Received 9 June 1998; accepted 14 October 1998

Abstract

We describe a novel modeling technique, based on Duhamel's theorem, to study the effects of time-varying winds on radon transport in soil near buildings. The technique, implemented in the model RapidSTART, reduces computational times for transient, three-dimensional, wind-induced soil-gas and radon transport by three to four orders of magnitude compared with conventional finite-difference models. To test model performance, we compared its predictions to analytical solutions of one-dimensional soil-column flow, finite-difference simulations of flow around a full-scale house, and measurements of transient soil–gas and radon entry into an experimental basement structure. These comparisons demonstrate that RapidSTART accurately simulates time-dependent radon transport through soil and its entry into buildings. As demonstrated in a previous study, steady winds can significantly affect radon entry. In this paper, we extend the findings of that study by applying RapidSTART to explore the impacts of fluctuating wind speed and direction on radon entry into a prototypical house. In soils with moderate to high permeability, wind fluctuations have a small to moderate effect on the soil-gas radon concentration field and entry rate into the building. Fluctuating wind direction dominates the impact on radon entry rates, while fluctuating wind speed has little effect. For example, in a soil with a permeability of 10^{-10} m^2, diurnal oscillations in wind direction can increase the predicted radon entry rate by up to 30% compared to steady-state predictions. © 1999 Elsevier Science Ltd. All rights reserved.

Keywords: Radon transport; Wind; Indoor air quality; Contaminant transport; Soil-gas transport; Duhamel's theorem; Modeling

*Corresponding author.

[1]Current address: Department of Mechanical Engineering, Carnegie Mellon, Pittsburgh, PA, USA.

1352-2310/99/$ - see front matter © 1999 Elsevier Science Ltd. All rights reserved.
PII: S1352-2310(98)00374-4

Nomenclature

C	soil-gas radon concentration (Bq m^{-3})
C_c	spatial average of the normalized radon concentration (–)
c_p	ground-surface pressure coefficient (–)
D	diffusion coefficient for radon in soil gas (m^2 s^{-1})
i	dummy variable of summation
j	dummy variable of summation
k	effective soil permeability (m^2)
l	length of the one-dimensional column (m)
L_c	characteristic length of the system (m)
M	number of ground-surface pressure fields and unit-step responses
n	dummy variable of summation
N	number of time steps
p	soil-gas disturbance pressure (Pa)
p_{-0}	amplitude of pressure signal (1 Pa)
p_{-A}	atmospheric pressure (Pa)
p_w	eave-height wind dynamic pressure (Pa)
S	radon source (Bq m^{-3} s^{-1})
t	time (s)
Δt	time step between successive simulation points (s)
$\boldsymbol{u}$	soil-gas bulk velocity (m s^{-1})
U	unit-step response (–)
V_e	eave-height wind speed (m s^{-1})
x, y, z	coordinates of a point in the soil block (m)

Greek letters

δ	pressure diffusivity (m^2 s^{-1})
ε	air-filled soil porosity (–)
λ	radon decay constant (2.098×10^{-6} s^{-1})
ρ	air density (kg m^{-3})
τ	dummy variable of integration
τ_c	characteristic time for the pressure field to r each steady state (s)
ξ	dummy variable of integration
μ	dynamic viscosity of air (kg m^{-1} s^{-1})
ω	frequency (s^{-1})

Note: (–) indicates a nondimensional variable.

1. Introduction

Indoor air exposures to soil-gas contaminants can cause large human health risks. Exposure to radon in indoor air is the single largest source of radiation exposure in the US general population (Nero, 1988). Advective entry of radon-bearing soil gas through cracks in the building substructure is the primary cause of elevated indoor concentrations (Nazaroff, 1992). By similar mechanisms, volatile organic compounds originating in hazardous waste sites and landfills can be transported into indoor air (Johnson and Ettinger, 1991; Little et al., 1992). To predict and control indoor-air exposures caused by soil-gas contaminants requires an understanding of the mechanisms responsible for gas-phase contaminant transport in near-surface soils.

Near buildings, the transport of gaseous contaminants through soil pores is strongly influenced by small pressure gradients. Pressure differences on the order of a few Pa can be induced across the building envelope by indoor–outdoor temperature differences, the operation of fans indoors, barometric pressure fluctuations, and wind. Efforts to model radon entry into buildings have primarily emphasized flows induced by steady-state pressure differences with uniform pressure on the ground surface (Bonnefous et al., 1992; Gadgil, 1992; Loureiro, 1990). Radon transport caused by time-dependent atmospheric pressure fluctuations have been studied recently (Robinson and Sextro, 1995; Robinson et al., 1996, 1997; Tsang and Narasimhan, 1992). An earlier investigation by Riley et al. (1996a) showed that the nonuniform pressure on the ground surface produced by steady winds can substantially influence predictions of soil-gas and radon entry into buildings.

In a pioneering study, Scott (1985) investigated radon transport in soils under conditions that included time varying winds. However, that investigation constrained the wind speed and direction to vary discretely on hourly intervals, thereby excluding the influence of short-term fluctuations. Their numerical model also ignored key features of radon's subsurface transport, including diffusion through the soil. Additionally, the investigators did not quantify the effect of the fluctuating wind on radon entry rates.

Riley (1996) summarized several modeling techniques available to predict soil-gas and radon entry rates into buildings. The most sophisticated of these – finite-difference and finite-element discretizations of the house and soil system – often require substantial simulation time. This requirement can be prohibitive for transient three-dimensional simulations, such as those necessary to examine the impacts of fluctuating winds on radon entry into buildings. In response to this problem, we have developed a technique for simulating time-dependent soil-gas and radon transport near buildings that utilizes Duhamel's theorem (Duhamel, 1833). The method is implemented in a model called RapidSTART (Rapid Simulation of Transient Air and Radon Transport). Depending on the soil permeability, RapidSTART can reduce simulation runtimes by three to four orders of magnitude compared to finite-difference simulations.

The purpose of this paper is to describe the development of RapidSTART and its exploratory application for studying radon entry into buildings. In the following sections, we first present the equations governing transient, three-dimensional soil-gas and radon transport. Next, results are summarized from a previous wind-tunnel study (Riley et al., 1996b) that quantified the

ground-surface pressure field (GSPF) generated by wind interacting with a building's superstructure. Duhamel's theorem is introduced in the context of soil-gas flow driven by fluctuating pressure boundary conditions, followed by a description of the theorem's discretization as applied in RapidSTART. Since real winds vary in both speed and direction, we also describe a method to simulate the impacts of fluctuating wind direction on soil-gas and radon transport. Finally, we describe the geometry of a prototypical house and the numerical space used in the simulations.

To test RapidSTART's performance, comparisons are made between the model's predictions and the results of three test cases: (1) the analytical solution of transient flow through a one-dimensional soil column, (2) simulation results from a transient finite-difference model of a full-scale house, and (3) experimental results of soil-gas and radon entry into an experimental structure. We then apply RapidSTART to three exploratory simulation scenarios, each with a wind signal chosen to elucidate the influence of fluctuations on the soil-gas radon concentration field and entry rate. The impact on radon entry rates is determined by making comparisons to steady-state predictions corresponding to the mean wind speed and direction.

2. Methods

2.1. Soil-gas pressure, velocity, and radon concentration equations

In this section we describe the equations governing soil-gas and radon transport. To determine the soil-gas pressure and velocity fields, we assume that the reference atmospheric pressure, p_A (Pa), remains constant over time and the hydrostatic and soil-gas disturbance pressures are much less than p_A. These assumptions give the continuity equation for soil gas (Riley, 1996):

$$\varepsilon \frac{\partial p}{\partial t} + p_A \nabla \cdot \boldsymbol{u} = 0, \tag{1}$$

where p is the soil-gas disturbance (gage) pressure (Pa), t is time (s), $\boldsymbol{u}$ is the soil-gas bulk velocity ($\mathrm{m\,s^{-1}}$), and ε is the air-filled porosity ($-$). Throughout this paper ($-$) indicates a nondimensional variable. For the simulations performed here, we assume that the soil-gas pressure and velocity are related via Darcy's law:

$$\nabla p = -\frac{\mu}{k}\boldsymbol{u}, \tag{2}$$

where μ is the dynamic viscosity of air ($\mathrm{kg\,m^{-1}\,s^{-1}}$) and k is the effective soil permeability (m^2). Eqs. (1) and (2) are linear, time-dependent relationships linking the soil-gas pressure and velocity fields. This linearity is important, since Duhamel's theorem applies only to linear systems.

The material conservation equation for radon in the soil gas is (Loureiro, 1990)

$$\frac{\partial}{\partial t}(C\varepsilon) = \nabla \cdot (D \nabla C) - \nabla \cdot (\boldsymbol{u} C) + \varepsilon(S - \lambda C), \tag{3}$$

where C is the soil-gas radon concentration ($\mathrm{Bq\,m^{-3}}$), S is the radon source term ($\mathrm{Bq\,m^{-3}\,s^{-1}}$), D is the diffusion coefficient for radon in soil gas ($\mathrm{m^2\,s^{-1}}$), and λ is the radon decay constant ($2.098 \times 10^{-6}\,\mathrm{s^{-1}}$).

2.2. Solution approach

We have solved these equations using two techniques: a conventional finite-difference model, called START, and a novel approach based on Duhamel's theorem, implemented in RapidSTART. START applies a modified SIMPLE algorithm (Patankar, 1980) for the spatial discretization of Eqs. (1)–(3), following Bonnefous et al. (1992), and a fully implicit temporal discretization. The solution approach is to first solve Eqs. (1) and (2), then use these results in the solution of Eq. (3). The pressure and velocity fields are calculated on staggered grids using an alternate direction implicit method; the concentration field is computed on the same grid as the pressure field. The spatial solution terminates when the computed pressure or concentration at each point changes fractionally by less than 1×10^{-6} between successive iterations. Details of the spatial and temporal discretization can be found in Riley (1996).

For three-dimensional transient simulations, such as those necessary to examine the impacts of wind on radon entry rates, START is very computationally expensive. Computing the soil-gas pressure and velocity fields dominates the simulation time. In RapidSTART, we apply Duhamel's theorem to accelerate the solution of Eqs. (1) and (2). Because the radon conservation equation does not respond linearly to changes in ground-surface pressures, Duhamel's theorem cannot be applied to solve Eq. (3). However, the use of conventional finite-difference modeling is satisfactory because solving Eq. (3) is much less computationally demanding than solving Eqs. (1) and (2).

2.3. Ground-surface pressure field (GSPF)

Wind interacting with a building superstructure creates a nonuniform pressure field on the ground surface that drives soil-gas movement. For the wind simulations presented here, we apply GSPF's measured in the U.C. Berkeley Architecture Department's wind tunnel facility (Riley et al., 1996b). In these 1 : 61 experiments, the house is a box with full-scale dimensions of $8.7\,\mathrm{m} \times 10.4\,\mathrm{m} \times 3\,\mathrm{m}$, and the atmospheric boundary layer corresponds to the wind field characteristic of a suburban area. Fig. 1 presents an example of the ground-surface pressure coefficient field, $c_p(x, y)$ (–), for the case of wind incident

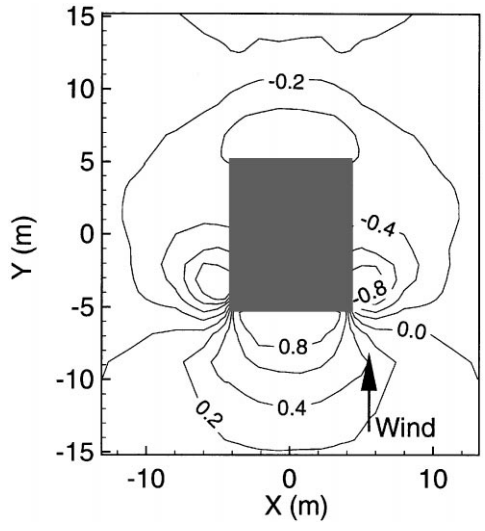

Fig. 1. Contour plot of the ground-surface pressure coefficient (plan view) for wind incident at an angle of 0° to the house. The pressure coefficient is the fraction of the eave-height (3 m) dynamic pressure of the wind that is felt on the ground surface. The contour interval is 0.2.

perpendicular to the short side of the house (wind incidence angle of 0°). We also measured the GSPF for wind incidence angles of 45° and 90°. The complex GSPF shown in Fig. 1 illustrates the need for three-dimensional simulations to investigate the effects of wind on soil-gas and radon entry rates.

The ground-surface pressure coefficient represents the fraction of the eave-height wind dynamic pressure that is felt on the soil surface:

$$p(x, y, z = 0, t) = p_w(t) c_p(x, y), \tag{4}$$

where x, y, and z are spatial coordinates (m); and $p_w(t)$ (Pa) is the eave-height wind dynamic pressure, defined as

$$p_w(t) = \frac{1}{2}\rho V_e(t)^2 . \tag{5}$$

Here, V_e is the time-dependent eave-height wind speed ($m\,s^{-1}$) and ρ is the air density ($kg\,m^{-3}$). Castro and Robins (1977) have shown that the pressure coefficient field remains constant for wind speeds greater than about $0.5\,m\,s^{-1}$.

Thus, given measured pressure-coefficient fields, $c_p(x, y)$, and time-dependent input on eave-height wind speed and direction, V_e, the time and position dependent pressure boundary condition at the ground surface is obtained from Eqs. (4) and (5). A pressure coefficient for the house relates the basement depressurization to $p_w(t)$ (Riley et al., 1996a).

In simulating a fluctuating atmospheric pressure ($p\_a(t)$ (Pa)), the ground surface boundary condition is:

$$p(x, y, z = 0, t) = p_a(t) \tag{6}$$

The basement pressure is also set to $p_a(t)$, based on the assumption of no time lag between the indoor and outdoor pressures.

2.4. Duhamel's theorem

The response of a linear system is proportional to the force driving the system. This property allows for two powerful solution techniques. First, the system's response to successive driving impulses can be computed as the sum of appropriately time-delayed responses to each impulse. Duhamel first applied this concept to study heat transport in solids (Duhamel, 1833; Myers, 1987). In electrical engineering, the analysis of linear circuits employs an analogous method, termed the "convolution integral" (Nilsson, 1984). We apply this idea to compute the soil-gas pressure field in the presence of fluctuating wind speed. Second, the system's response to a complex driving force can be computed as the sum of the responses to simpler driving forces which sum to the original driving force. In RapidSTART we apply this property to simulate the impact of fluctuating wind direction on the soil-gas pressure field.

Duhamel's theorem has been applied to investigate transient groundwater flow. Weeks (1979) successfully employed a version of the theorem to explain the impacts of barometric pressure fluctuations on wells in deep, unconfined aquifers. Moench et al. (1974) used the method to predict variations in a perennial stream interacting with an aquifer. They showed good agreement between modeled and experimental observations of the stream-aquifer system. Pinder et al. (1969) applied the theorem to determine the diffusivity of an aquifer in Nova Scotia. Comparisons to experimental data from pumping tests showed good agreement with their modeling results. In parallel with the efforts described in this paper, Duhamel's theorem has successfully been employed to examine the impacts of atmospheric pressure fluctuations on soil-gas entry into an experimental basement structure (Robinson et al., 1996, 1997). To our knowledge, the work presented here represents the first time Duhamel's theorem has been applied to simulate subsurface contaminant transport.

Duhamel's theorem, applied to the case of a fluctuating, wind-induced GSPF (known via $p_w(t)$), states that the soil-gas pressure field can be represented as

$$p(x, y, z, t) = \int_0^t U(x, y, z, t - \tau)\frac{dp_w}{d\tau}\,d\tau, \tag{7}$$

where the normalized unit-step response, $U(x, y, z, t)$ ($-$), characterizes the soil-gas pressure field's time-dependent behavior in response to a step change from 0 to 1 Pa of $p_w(t)$, and τ is a dummy variable of integration. In particular, U (x, y, z, t) is the time history of the soil-gas

pressure field (normalized by 1 Pa) after a discrete change from 0 to 1 Pa of the parameter defining the pressure boundary condition (p_w or p_a). Eq. (7) represents the first of the linear superposition properties discussed earlier. For simulations considering a fluctuating atmospheric pressure, p_w is replaced by p_a in Eq. (7).

Note that Eq. (7) permits only continuous temporal changes in the pressure boundary conditions. The discretized version of this equation, described in the following subsections, provides a method to simulate discrete changes in the boundary conditions, as well as changes associated with shifts in wind direction.

2.5. Discretization of Duhamel's theorem

To implement Duhamel's theorem in RapidSTART, we divide the integral in Eq. (7) into discrete time steps and assume a constant time rate of change of the wind dynamic pressure during each time step:

$$p(x,y,z,t) = \sum_{j=0}^{N-1} \left\{ \int_{t-(j+1)\Delta t}^{t-j\Delta t} \left[\left. \frac{\partial p_w}{\partial t} \right|_j \right] \times U(x,y,z,t-\tau)\,\mathrm{d}\tau \right\}. \quad (8)$$

Here, Δt (s) is the time step between successive simulation points (we choose Δt based on the soil-gas pressure field's response time and the characteristics of the fluctuating wind), j is a dummy variable of summation, $N(=t/\Delta t)$ represents the number of time steps from 0 to t, and $\partial p_w/\partial t|_j$ is evaluated at the time $t-(j+1/2)\Delta t$. We evaluate Eq. (8) with a linear, trapezoidal integration scheme.

2.6. Simulating a fluctuating wind direction

Simulations with a varying wind direction employ the GSPF's determined in Riley et al. (1996b) for wind-incidence angles of 0°, 45°, and 90°. Ideally, unit-step responses would be generated for more than three wind-incidence angles, based on additional wind-tunnel or numerical experiments. Here we formulate the technique to simulate a fluctuating wind direction for an arbitrary number of GSPF's (i.e., an arbitrary number of bins into which the wind direction signal has been divided) and unit-step responses. Eq. (9) applies the second property of linear superposition discussed above for the case where the wind direction has been separated into M bins (note the similarity to Eq. (8)):

$$p(x,y,z,t) = \sum_{i=1}^{M} \sum_{j=0}^{N-1} \left\{ \int_{t-(j+1)\Delta t}^{t-j\Delta t} \left[\left. \frac{\partial p_{w,i}}{\partial t} \right|_j \right] \times U_i(x,y,z,t-\tau)\,\mathrm{d}\tau \right\} \quad (9)$$

where i is a dummy variable of summation and also references, as a subscript, the wind direction for $\partial p_w/\partial t$ and U. In Eq. (9), i acts as a switch to indicate which of the unit-step responses are applied in the summation for any particular time period. For the cases presented in this paper, the wind direction varies within a 135° range and there are three GSPF's. Therefore, $i = 1$, 2, and 3 correspond to wind-incidence angles of 0°, 45°, and 90°, respectively. The second property of linear superposition discussed above also allows for simulations that simultaneously include varying atmospheric pressure, wind speed, and wind direction.

The soil-gas pressure field at a particular time depends on both the current wind direction and speed, and, if the wind has been from another direction in the near past (i.e., less than several times the characteristic response time of the system), that wind direction and speed. The characteristic time, τ_c (s), for the pressure field to reach steady state after a perturbation is (Nazaroff, 1992)

$$\tau_c = \frac{L_c^2}{\delta}, \quad (10)$$

where L_c is a characteristic length (m) of the system and δ ($\mathrm{m^2\,s^{-1}}$) is the pressure diffusivity, defined as $\delta = kp_A/\varepsilon\mu$. We take L_c to be 15 m, equivalent to half the horizontal extent of the soil block. For a soil permeability of $10^{-8}\,\mathrm{m^2}$, τ_c is about 2 s. Therefore, if the wind direction changes from 0° to 45°, the influence of the unit-step response corresponding to 0° will essentially be nil after several characteristic times, or about 10 s. The characteristic time varies inversely with soil permeability, so, for a soil permeability of $10^{-10}\,\mathrm{m^2}$, the soil-gas pressure field requires about 1000 s to stabilize after the wind direction has shifted.

Earlier studies that applied Duhamel's theorem to groundwater transport problems either computed an analytical solution of or measured the unit-step response for a single output variable of the system. In our application, the finite-difference model START is used to determine the unit-step response of the soil-gas pressure for each grid cell in the computational domain. Although significant simulation time is needed to generate the unit-step response, this requirement is much less demanding than the computational constraint posed by performing three-dimensional transient simulations with START. Using the stored unit-step response, RapidSTART computes the soil-gas pressure at every time step using Eq. (9), replacing START's solution of Eqs. (1) and (2).

2.7. House geometry and numerical space

For exploratory applications of RapidSTART, we chose a modeled house geometry that is typical of a single-family structure in size and shape. The building

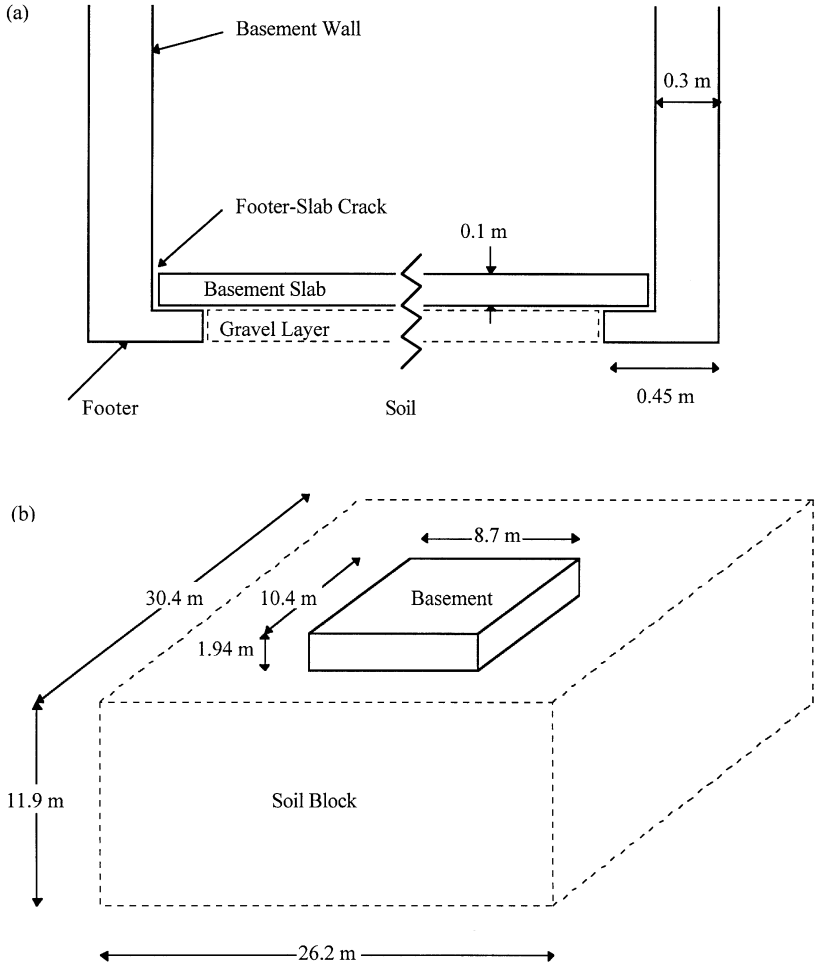

Fig. 2. Geometry of the substructure of the (a) house cross section and (b) computational space. The diagrams are not to scale.

has a plan area of 8.7 m × 10.4 m; the basement and footers represent standard construction practice and are depicted in Fig. 2a. A 1 mm L-shaped perimeter crack provides the route for radon entry into the basement. This type of shrinkage crack is common in buildings with basements. The soil-gas pressure, velocity, and concentration fields were computed in a soil block that measures 30.4 m × 26.2 m horizontally, and extends 11.9 m below the soil surface (Fig. 2b). There are 40 716 node points in this volume. The exterior surfaces of the soil block are taken to be Neumann boundaries (no flow), as are all interfaces between the soil and basement. The Neumann boundary at the bottom of the computational space represents an impermeable layer at this depth (e.g., the water table). (Unpublished simulation results show that predictions of radon entry for steady driving forces are relatively insensitive to the depth of the impermeable layer if it is much larger than the basement depth.) Dirichlet boundaries (fixed pressure) are imposed on the ground surface and along the crack that connects the sub-slab gravel layer with the basement. In contrast to the pressure field computations, we represent the ground surface in the concentration field simulation by a mixed boundary condition because there may be areas (i.e., on the leeward side of the house) where comparable advective and diffusive radon effluxes exist.

2.8. Solution procedure

Fig. 3 describes the four-step procedure we use to compute the radon entry rate into the building in the presence of fluctuating pressure boundary conditions. First, the finite-difference model START computes the unit-step response of the soil-gas pressure field (once computed for a given house geometry and set of wind directions, this unit-step response can be used to simulate

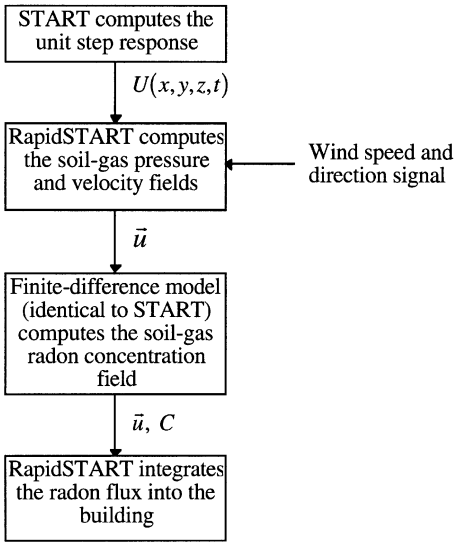

Fig. 3. Schematic of the RapidSTART simulation procedure.

the transient soil-gas pressure and velocity fields for any input wind or atmospheric pressure signal). RapidSTART then applies Duhamel's theorem to compute the soil-gas pressure and velocity fields for the imposed pressure boundary conditions, as defined by the time-varying wind speed and direction, or atmospheric pressure signals. Third, using the soil-gas velocity field as input, START calculates the soil-gas radon concentration field. Finally, integrating the radon flux over the length of the footer-slab crack yields the radon entry rate into the building.

3. Model testing

Test Case 1: *Analytical solution for one-dimensional transport*. The first test case compares RapidSTART predictions to analytical solutions of the transient soil-gas pressure field in a one-dimensional column. The pressure field is defined by the one-dimensional form of Eqs. (1) and (2), with the following boundary and initial conditions:

$$\frac{p(0,t)}{p_o} = \sin(\omega t), \quad t > 0, \tag{11}$$

$$p(l,t) = 0, \quad t > 0, \tag{12}$$

$$p(x,0) = 0, \quad 0 \leqslant x \leqslant l, \tag{13}$$

where p_0 is the amplitude of the pressure signal (1 Pa), l is the length of the column (2 m) and ω is the frequency of the fluctuating boundary condition (chosen to be 0.105 s^{-1}, equivalent to a period of 60 s).

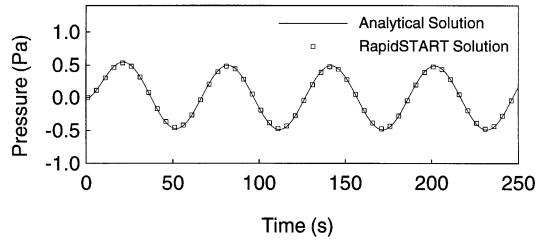

Fig. 4. Comparison of analytical and numerical predictions of the soil-gas disturbance pressure at 37.5 cm in the soil column. The soil permeability is 10^{-12} m^2 (test case 1).

Carslaw and Jaeger (1959, p. 104) give the solution to Eqs. (1) and (2) subject to the boundary conditions given in Eqs. (11)–(13) as

$$\frac{p(x,t)}{p_0} = \frac{2\delta\pi}{l^2}\sum_{n=1}^{\infty} n \exp\left(-\frac{\delta n^2\pi^2 t}{l^2}\right)\sin\left(\frac{n\pi x}{l}\right) \times \int_0^t \exp\left(\frac{\delta n^2\pi^2\xi}{l^2}\right)\sin(\omega\xi)\mathrm{d}\xi, \tag{14}$$

where n and ξ are dummy variables of summation and integration, respectively.

Fig. 4 shows excellent agreement between RapidSTART's predictions and the analytical solution of the pressure 0.375 m from the column's end for a case in which the soil permeability is 10^{-12} m^2. Simulations also generated excellent agreement for soil permeabilities of 10^{-8} and 10^{-10} m^2 and for driving pressures with periods ranging from 1 to 300 s. These results demonstrate that RapidSTART can accurately predict the transient soil-gas pressure field for fluctuating boundary conditions typical of those near houses.

Test Case 2: *Comparison of RapidSTART to START*. Test Case 2 compares simulation results from RapidSTART to the finite-difference model START for the case of a fluctuating wind incident on a two-dimensional section of the house described in Fig. 2. This case explores whether RapidSTART's simulation of the soil-gas pressure field matches the finite-difference solution upon which the unit-step response is based. The fluctuating wind dynamic pressure was prescribed to be sinusoidal, with a mean and amplitude of 1 Pa, and a period of 2 s.

Fig. 5 compares the predicted soil-gas and normalized radon entry rates from RapidSTART and START for a soil permeability of 10^{-10} m^2; not shown is an analogous test for a soil permeability of 10^{-8} m^2. The radon entry rate into the basement is normalized by the deep-soil radon concentration. Results for both permeabilities demonstrate excellent agreement between the two models. Significantly, for this two-dimensional case,

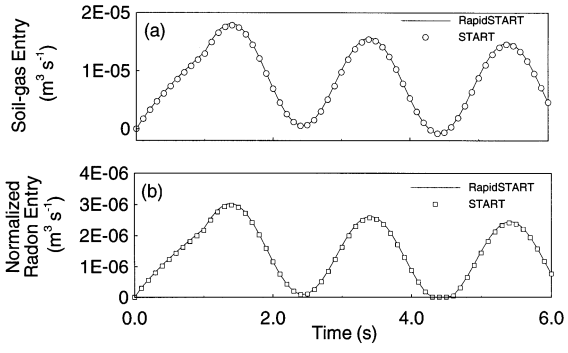

Fig. 5. Comparison between RapidSTART and START predictions of the (a) soil-gas and (b) normalized radon entry rates for a fluctuating wind signal and a soil permeability of 10^{-10} m^2 (test case 2). The normalized radon entry rate is the radon entry rate into the basement divided by the deep-soil radon concentration.

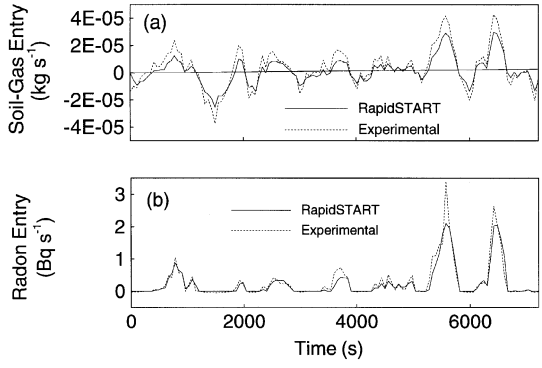

Fig. 6. RapidSTART predictions and measurements from the Small Structures experiment of the (a) soil-gas and (b) radon entry rates (test case 3). Negative entry rates indicate flow into the structure.

RapidSTART reduced simulation runtimes for the 10^{-8} m^2 soil from 2 h to 20 s (a factor of 360), and from 20 h to 20 s (a factor of 3600) for the 10^{-10} m^2 soil. These simulations were performed on a Hewlett Packard 9000/735s running at 99 MHz.

Test Case 3: *Experimental test of RapidSTART*. The third test case compares RapidSTART predictions to measurements of radon and soil-gas entry into the Small Structures Facility in the Santa Cruz Mountains. These measurements were made during a study of the impacts of fluctuating atmospheric pressures on radon entry rates (Robinson and Sextro, 1997). Fisk et al. (1992) describe the basement structure, instrumentation, and soil properties at the facility. Briefly, the experimental structure has a depth of 2.25 m, a horizontal cross-section of 1.17×1.75 m^2, and, to reduce the impacts of wind, a shallow (0.2 m) above-ground profile. Soil-gas and radon enter through a 4 cm diameter hole in the center of the footer slab.

The permeability of the soil surrounding the structure and the gravel directly beneath it were taken to be 3×10^{-11} m^2 and 2×10^{-8} m^2, respectively; the soil porosity is 0.4 (Garbesi et al., 1996). We use the measured deep-soil radon concentration of 115 000 Bq m^{-3} to determine S. In the model, 13 800 control volumes define the soil block and basement structure, and the time step is 60 s. The simulation begins with soil-gas pressure and radon concentration fields that correspond to the steady-state solution for zero disturbance pressure at the ground surface and basement crack. Over time, fluctuating atmospheric pressures drive soil-gas and radon into and out of the structure.

Fig. 6 shows RapidSTART's predictions and the experimental results for the soil-gas (a) and radon (b) entry rates into the experimental basement. The integrated absolute difference between the experimental and simulated radon entry rates over the 2 h simulation is only 14%, and the measured time-dependence of radon entry is well described by the model. These results demonstrate RapidSTART's ability to accurately simulate transient soil-gas and radon transport and entry into buildings under field conditions.

4. Effects of transient winds on radon entry

In this section we describe three exploratory scenarios that examine the effects of fluctuating wind direction and speed on radon entry rates for soil permeabilities of 10^{-8} and 10^{-10} m^2 (see Table 1). These permeabilities are near or beyond the high end of expected values around most single-family houses (Garbesi et al., 1996; Nazaroff, 1992). However, 10^{-10} m^2 is a reasonable permeability for homes in Spokane, WA. We chose Spokane as a reference because radon entry and mitigation has been investigated in several houses in the area (Fisk et al., 1995; Turk et al., 1990). For soils with smaller permeabilities, the time required to generate the unit-step response and associated storage requirements can be large. Riley (1996) presents a technique to reduce the storage requirements by curve-fitting the time history of the unit-step response. Our motivation in using the relatively high permeabilities discussed here is to demonstrate the capabilities of RapidSTART and to investigate the impacts of transient winds on radon entry rates in relatively loose soils, where the effects of steady winds are the greatest.

4.1. Exploratory scenario 1: fluctuating wind speed

In exploratory scenario 1, we consider a wind whose speed oscillates sinusoidally in time, but whose direction

Table 1
The three RapidSTART exploratory scenarios

Scenario	Description	Permeability	Wind
1	Fluctuating wind speed	10^{-8} and 10^{-10} m^2	• Mean speed = 3.6 m s^{-1} • Amplitude = 0.57 m s^{-1} • Frequency = 0.024 s^{-1} • Incidence angle = 0°
2	Diurnally oscillating wind signal	10^{-10} m^2	• Speed = 3.6 m s^{-1} • Incidence angle of 0° for 12 h, followed by an incidence angle of 180° for 12 h
3	Measured wind signal (9000 s) from the Richmond Field Station with variable speed and direction	10^{-8} m^2	• Mean speed = 5.1 m s^{-1} • Mean incidence angle = 201°

is fixed. The characterization of the atmospheric boundary layer presented by Teunissen (1980) is used to generate an artificial wind speed signal. The wind-incidence angle in these simulations is held constant at 0°, and the mean-wind speed is 3.6 m s^{-1} (the 50th percentile wind speed for Spokane, Washington, over a period of 25 years (NOAA, 1980)). The peak in the wind-speed power spectrum of Teunissen's "modified Kaimal model" occurs at a speed of 0.57 m s^{-1} and a frequency, ω, of 0.024 s^{-1}. We represent the wind dynamic pressure signal as

$$p_w(t) = \frac{1}{2}\rho(3.6 + 0.57\sin(2\pi\omega t))^2. \quad (15)$$

The model results show that for soil permeabilities of 10^{-8} and 10^{-10} m^2 the time-averaged radon entry rate with the input wind signal defined by Eq. (15) is about 1% higher than the entry rate for a constant wind speed of 3.6 m s^{-1}. Because the soil-gas pressure field responds linearly to the fluctuating pressure boundary condition, the time-averaged soil-gas flow into the building is the same for the fluctuating and steady wind cases. The small change in radon entry rate indicates that the radon concentration field near the entry points of the building is largely unaffected by the fluctuating pressure boundary condition. These results demonstrate that wind speed fluctuations characteristic of the peak in the wind speed power spectrum have negligible impact on the radon entry rate if the wind direction is steady.

4.2. Exploratory scenario 2: diurnally oscillating wind direction

Exploratory scenario 2 investigates the impacts on the radon entry rate of a wind signal that oscillates diurnally between wind-incidence angles of 0° and 180°. The input wind signal for this simulation has a constant speed of 3.6 m s^{-1} and an incidence angle of 0° for 12 h, followed by the same wind speed with an incidence angle of 180° for the next 12 h. This scenario imitates wind conditions characteristic of coastal regions, and illustrates the impacts of large, periodic changes in wind direction. The initial condition for this simulation was the steady state response to a constant wind speed of 3.6 m s^{-1} at an incidence angle of 0°.

Fig. 7 shows a 10-day history of the (a) wind direction and (b) radon entry rate into the basement driven by the diurnally oscillating wind (the soil permeability is 10^{-10} m^2). Also shown (c) is C_c (—), the spatial average of the normalized radon concentration in a plane surface bounded by the lower interior edges of the footers. In Fig. 7b and c the dashed lines represent the radon entry rate

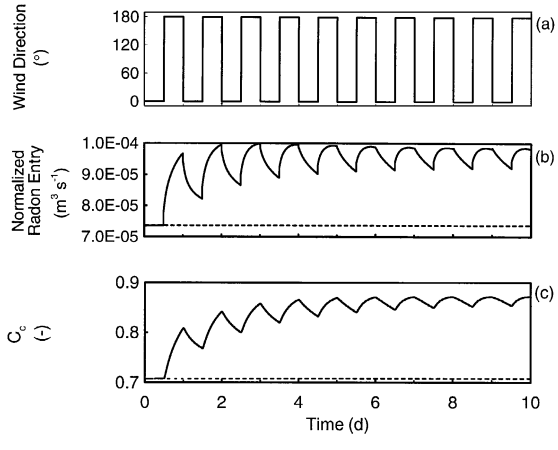

Fig. 7. (a) wind direction, (b) predicted normalized radon entry rate, and (c) C_c for a constant wind speed, a diurnally oscillating wind direction, and a soil permeability of 10^{-10} m^2 (exploratory scenario 2). The normalized radon entry rate is the radon entry rate into the basement divided by the deep-soil radon concentration. The dashed lines represent steady-state values corresponding to a 3.6 m s^{-1} wind incident at 0°.

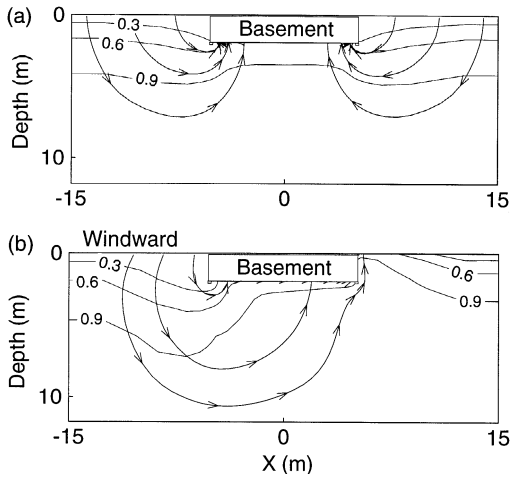

Fig. 8. Normalized soil-gas radon concentration field and streamlines for cases with (a) no wind and (b) a 3.6 m s^{-1} wind incident at 0°. The basement depressurization is -2.0 Pa and the soil permeability is 10^{-10} m^2 for both cases. The figure represents concentrations in a vertical plane bisecting the basement parallel to the long side of the house and the wind. Notice the enrichment of soil-gas radon on the leeward side of the house in (b) as compared to (a).

and the value of C_c, respectively, corresponding to a steady wind incidence angle of 0° and speed of 3.6 m s^{-1}. The diurnally oscillating wind direction caused a 30% increase in the average radon entry rate into the basement compared to the steady-state case. The soil-gas entry rate was unaffected by the oscillating wind.

Fig. 7c indicates that the source of radon available for entry into the basement increased over the 10-day simulation period. This enrichment of the soil-gas radon concentration near the footers occurs because, during each 12 h period, the wind-induced soil-gas flow moves radon from deep in the soil profile towards the soil surface on the leeward side of the house. We illustrate this effect in Fig. 8, which shows the steady-state soil-gas radon concentration field and streamlines for cases with (a) basement depressurization but no wind, and (b) a 3.6 m s^{-1} wind, incident at 0°. Notice the enrichment of soil-gas radon on the leeward side of the basement in the case with wind (b) as compared to the case without wind (a). Riley et al. (1996a) discuss this feature of steady-state wind-induced soil-gas radon flow in detail. As the wind shifts 180° in direction, the streamlines shown in Fig. 8b are mirrored about the $x = 0$ line, and originate on the right-hand side of the basement. This transition takes place over several characteristic soil-gas pressure response times, or about 10^3 s for a soil permeability of 10^{-10} m^2, as described above. Once this transition has occurred, radon from the enriched zone is forced back under the basement, resulting in an increase in the time-averaged radon concentration near the building's entry points. The radon entry rate rises as a result of this increased radon source. Scenario 2 illustrates that a diurnally fluctuating wind direction can enhance the subslab radon concentration, thereby increasing radon entry into the building.

4.3. Exploratory scenario 3: actual transient wind signal

In exploratory scenario 3, we perform a RapidSTART simulation with a wind signal collected as part of a full-scale radon mitigation experiment at the Richmond Field Station (RFS) in Contra Costa County, CA. A weather station (Belfort, 1997) placed 7 m above the ridge of the test house's roof measured wind speed and direction. The average wind speed and direction over the 2.5 h period are 5.1 m s^{-1} and 201°, respectively. The wind direction signal is divided into three 45° bins with incidence angles centered on 0°, 45°, and 90°. We use the center of each bin (0°, 45°, or 90°) as the wind incidence angle defining the bin. For scenario 3, the house is oriented such that the average wind incidence angle is 45°. With this configuration, the wind has incidence angles of 0°, 45°, and 90° for 12%, 71%, and 17% of the simulation period, respectively. The simulations begin with ground-surface pressure, soil-gas pressure, and soil-gas concentration fields equivalent to the steady-state solution for a 5.1 m s^{-1} wind incident at 45°; the soil permeability is 10^{-8} m^2.

Fig. 9 presents a portion of the RFS wind (a) direction and (b) speed signals, and the predicted (c) soil-gas and (d) radon entry rates for this scenario. In Fig. 9a and b the dashed lines represent the average wind direction and speed over the 2.5 h simulation period, respectively. The dashed lines in Fig. 9c and d represent the predicted steady-state soil-gas and radon entry rates, respectively, corresponding to this average wind speed and direction.

The time-averaged normalized radon entry rate for the transient simulation is 21% larger than the steady-state radon entry rate corresponding to the average wind speed and direction. This increase is predominantly due to the larger steady-state soil-gas entry rates for wind-incidence angles of 0° and 90°, as compared to 45°. Thus, for times when the wind is from either 0° or 90°, a larger driving force for radon entry exists in the transient case than in the steady-state case, which assumes a constant incidence angle of 45°. This simulation indicates that the orientation of the house with respect to the average wind direction and the fraction of time that the wind comes from the average direction affects the comparison between the transient and steady-state cases.

5. Conclusions

Our application of Duhamel's theorem in RapidSTART represents a novel and efficient method of

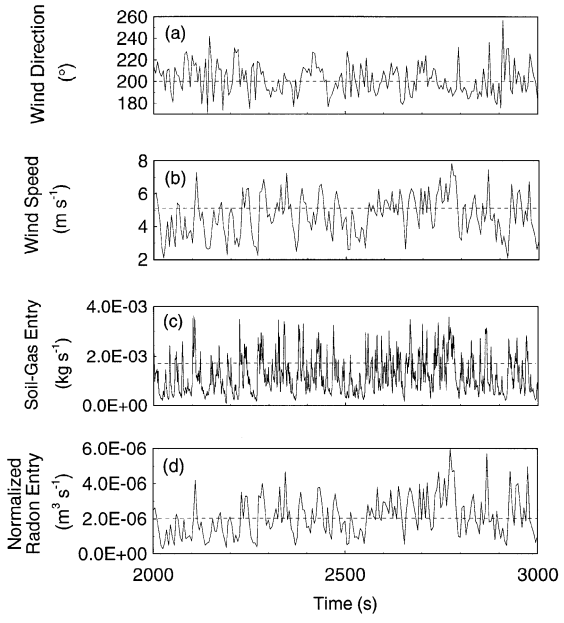

Fig. 9. A portion of the (a) wind speed, (b) wind direction, and predicted (c) soil-gas and (d) normalized radon entry rates for the RFS wind signal (exploratory scenario 3). The normalized radon entry rate is the radon entry rate into the basement divided by the deep-soil radon concentration. The dashed lines represent steady values corresponding to the average wind speed and direction over the 2.5 h simulation.

simulating transient soil-gas and contaminant flow under spatially heterogeneous, transient boundary conditions. In contrast to previous applications of Duhamel's theorem, details of the flow and concentration fields are calculated at each time step. Depending on soil permeability, RapidSTART reduces the computational time required for three-dimensional simulations by three to four orders of magnitude compared to standard finite-difference approaches. RapidSTART performed well in three test cases, including a comparison with experimental measurements from a well-characterized basement structure.

We performed three sets of simulations to illustrate the effects of fluctuating winds on radon entry into houses. The first set of simulations considered the effect of a sinusoidally oscillating wind speed on the radon entry rate. The results suggested that fluctuations in the wind speed typical of the peak in the power spectrum have a negligible impact on the radon entry rate. The second set of simulations considered a constant speed wind signal that oscillated 180° in direction on a diurnal cycle. This wind signal increased the time-averaged radon entry rate by about 30% relative to a steady wind. The third set of simulations investigated the impacts of a real fluctuating wind signal on radon entry rates considering changes in both wind speed and direction. The time-averaged radon entry rate increased in this case by 21% over the steady-state prediction.

These results suggest that a fluctuating wind direction can affect radon entry rates by either altering the soil-gas radon concentration field or the soil-gas entry rate into the building. Fluctuating wind speed alone has a negligible effect on the radon entry rate. This study also provides insight into the expected magnitude of the effect of transient winds on radon entry into buildings. For the relatively permeable soils tested here, the overall effect of the fluctuating components of wind on radon entry rates is small to moderate. The impact of fluctuating winds on radon entry in less permeable soils remains unresolved.

In the context of wind-induced soil-gas and radon transport, the use of RapidSTART has made the analysis of transient winds tractable. Additionally, because the methods employed in RapidSTART are general, we expect that the modeling approach can be applied productively to other environmental systems subject to transient boundary conditions. For example, the transport and entry into buildings of other soil-gas contaminants (e.g., VOCs) could be examined using the techniques employed in RapidSTART.

Acknowledgements

This work was supported by the Assistant Secretary for Conservation and Renewable Energy and by the Director, Office of Energy of the US Department of Energy under Contract No. DE-AC03-76SF00098.

References

Belfort, 1997. Belfort Instrument Co., Bulletin 118. Baltimore, MD.

Bonnefous, Y.C., Gadgil, A.J., Fisk, W.J., Prill, R.J., Nematollahi, A.R., 1992. Field study and numerical simulation of subslab ventilation systems. Environmental Science and Technology 26, 1752–1759.

Carslaw, H.S., Jaeger, J.C., 1959. Conduction of Heat in Solids. Clarendon Press, Oxford.

Castro, I.P., Robins, A.G., 1977. The flow around a surface-mounted cube in uniform and turbulent streams. Journal of Fluid Mechanics 79, 307–335.

Duhamel, A., 1833. Memoire sur la methode general relative au movement de la chaleur dans les corps solides plonges dans les milieux dont la temperature varie avec le temps. Journal of Ec. Polyt. Paris 14, 20.

Fisk, W.J., Modera, M.P., Sextro, R.G., Garbesi, K., Wollenberg, H.A., Narasimhan, T.N., Nuzum, T., Tsang, Y.W., 1992. Radon entry into basements: approach, experimental structures, and instrumentation of the small structures project. LBL–31864, Lawrence Berkeley National Laboratory, Berkeley, CA.

Fisk, W.J., Prill, R.J., Wooley, J., Bonnefous, Y.C., Gadgil, A.J., Riley, W.J., 1995. New methods of energy efficient radon mitigation. Health Physics 68, 689–698.

Gadgil, A.J., 1992. Models of radon entry. Radiation Protection Dosimetry 45, 373–380.

Garbesi, K., Sextro, R.G., Robinson, A.L., Wooley, J.D., Owens, J.A., Nazaroff, W.W., 1996. Scale dependence of soil permeability to air: measurement method and field investigation. Water Resources Research 32, 547–560.

Johnson, P.C., Ettinger, R.A., 1991. Heuristic model for predicting the intrusion rate of contaminant vapors into buildings. Environmental Science and Technology 25, 1445–1452.

Little, J.C., Daisey, J.M., Nazaroff, W.W., 1992. Transport of subsurface contaminants into buildings. Environmental Science and Technology 26, 2058–2066.

Loureiro, C.O., 1990. Three-dimensional simulation of radon transport into houses with basements under constant negative pressure. Environmental Science and Technology 24, 1338–1348.

Moench, A.F., Sauer, V.B., Jennings, M.E., 1974. Modification of routed streamflow by channel loss and base flow. Water Resource Research 10, 963–968.

Myers, G.E., 1987. Analytical Methods in Conduction Heat Transfer. Genium Publishing Corporation, Schenectady, NY.

Nazaroff, W.W., 1992. Radon transport from soil to air. Reviews of Geophysics 30, 137–160.

Nero, A.V., 1988. Radon and its decay products in indoor air : an overview. In: Nazaroff, W.W., Nero, A.V. (Eds.), Radon and Its Decay Products in Indoor Air. Wiley, New York, pp. 1–53.

Nilsson, J.W., 1984. Electric Circuits. Addison-Wesley Publishing Co., Reading, MA.

NOAA, 1980. Local climatological data, annual summaries for 1980, Part II – NEB-WYO. National Climatic Center, National Oceanic and Atmospheric Administration, Asheville, NC.

Patankar, S.V., 1980. Numerical Heat Transfer and Fluid Flow. Hemisphere Publishing, New York, NY.

Pinder, G.F., Bredehoeft, J.D., Cooper, H.J., 1969. Determination of aquifer diffusivity from aquifer response to fluctuations in river stage. Water Resource Research 5, 850–855.

Riley, W.J., 1996. Wind-induced contaminant transport in near-surface soils with application to radon entry into buildings, Ph.D. Thesis, U.C. Berkeley, 266 pp.

Riley, W.J., Gadgil, A.J., Bonnefous, Y.C., Nazaroff, W.W., 1996a. The effect of steady winds on radon-222 entry from soil into houses. Atmospheric Environment 30, 1167–1176.

Riley, W.J., Gadgil, A.J., Nazaroff, W.W., 1996b. Wind-induced ground-surface pressures around a single-family house. Journal of Wind Engineering and Industrial Aerodynamics 61, 153–167.

Robinson, A.L., Sextro, R.G., 1995. Direct measurements of soil-gas entry into an experimental basement driven by atmospheric pressure fluctuations. Geophysical Research Letters 22, 1929–1932.

Robinson, A.L., Sextro, R.G., 1997. Radon entry into buildings driven by atmospheric pressure fluctuations. Environmental Science and Technology 31, 1742–1748.

Robinson, A.L., Sextro, R.G., Fisk, W.J., 1996. Soil-gas entry into an experimental basement driven by atmospheric pressure fluctuations – measurements, spectral analysis, and model comparison. Atmospheric Environment 31, 1477–1485.

Robinson, A.L., Sextro, R.G., Riley, W.G., 1997. Soil-gas entry into houses driven by atmospheric pressure fluctuations – the influence of soil properties. Atmospheric Environment 31, 1487–1495.

Scott, A.G., 1985. A computer model study of soil gas movement into buildings. Report No. 1389/1333, Department of Health and Welfare, Ottawa, Canada.

Teunissen, H.W., 1980. Structure of mean winds and turbulence in the planetary boundary layer over rural terrain. Journal of Wind Engineering and Industrial Aerodynamics 6, 188–221.

Tsang, Y.W., Narasimhan, T.N., 1992. Effects of periodic atmospheric pressure variation on radon entry into buildings. Journal of Geophysical Research –Solid Earth 97, 9161–9170.

Turk, B.H., Prill, R.J., Grimsrud, D.R., Moed, B.A., Sextro, R.G., 1990. Characterizing the occurrence, sources, and variability of radon in Pacific Northwest homes. Journal of Air Waste Management Assoc. 40, 498–506.

Weeks, E.P., 1979. Barometric fluctuations in wells tapping deep unconfined aquifers. Water Resource Research 15, 1167–1176.